

**FLEXURAL VIBRATIONS OF A BEAM ON PERIODICALLY
ARRANGED EXTERNAL SUPPORTS AND PARTIALLY COATED BY
PIEZOELECTRIC PATCH**

Ara S. Avetisyan, Karen B. Ghazaryan, Pier Marzocca

Keywords: free vibrations, piezoelectric patch, matrix method, harvesting energy, electrical voltage generating, localization.

Аветисян Ара С., Казарян Карен Б., Марзокка Пьер

**Изгибные колебания частично покрытой пьезоэлектрической накладкой балки,
опирающейся на периодически расположенные внешние опоры**

Ключевые слова: свободные колебания, пьезоэлектрический накладной элемент, матричный метод, накопление энергии, генерация электрического напряжения, локализация.

Рассматриваются свободные колебания балки, часть балки опирается на периодически расположенные внешние опоры и частично покрыта идеально приклеенной пьезоэлектрической накладкой. На основе теории балок Эйлера–Бернулли и метода матрицы переноса получены общие решения в периодической части балки. Показано, что при совпадении собственных частот свободных колебаний балки с полосой запретных частот соответственной бесконечной балки, происходит сильная локализация наклонов и моментов балки на первом интерфейсе периодической части балки. Электрическое напряжение, генерируемое пьезоэлектрической накладкой, пропорционально наклонам периодической структуры балки. Максимальное накопление энергии происходит на собственных частотах в полосе частот задерживания, при которых происходит сильная локализация наклона балки.

Արա Ս. Ավետիսյան, Կարեն Բ. Ղազարյան, Պիեր Մարզոկա

**Պարբերաբար դասավորված արտաքին հենարանների վրա հենվող մասնակիորեն
ծածկված պիեզոէլեկտրական վերդիրով հեծանի ծռման տատանումները**

Հիմնաբառեր ազատ տատանումներ, պիեզոէլեկտրական վերդիր, մատրիցային մեթոդ, էներգիայի կուտակում, էլեկտրական լարման առաջացում, տեղայնացում:

Դիտարկվում է հեծանի ազատ տատանումները: Հեծանը մի մասով հենվում է պարբերաբար տեղակայված արտաքին հենարանների վրա և մասամբ ծածկված է կատարյալ սոսնձված պիեզոէլեկտրական վերդիրով: Հեծանի պարբերական հենարաններով մասում ընդհանուր լուծումները ստացվում են Էյլերի-Բեռնուլլիի ճառագայթի տեսության և փոխանցման մատրիցի մեթոդի հիման վրա: Ցույց է տրվում, որ երբ հեծանի ազատ տատանումների սեփական հաճախականությունները համընկնում են համապատասխան անվերջ հեծանի արգելված հաճախականությունների գոտու հետ, հեծանի պարբերական մասի առաջին միջերեսում տեղի է ունենում հեծանի ծռման թեքությունների և մոմենտների ուժեղ տեղայնացում: Պիեզոէլեկտրական ծածկույթում առաջացած էլեկտրական լարումը համեմատական է հեծանի պարբերական կառուցվածքում առաջացող թեքություններին: Էներգիայի առավելագույն կուտակումը տեղի է ունենում արգելման գոտում սեփական հաճախականություններում, որոնց դեպքում տեղի է ունենում հեծանի ծռման թեքության ուժեղ տեղայնացում:

A beam flexural vibrations are considered, part of the beam rests on periodically located external supports and is partially covered with a perfectly glued piezoelectric patch. Based on the Euler–Bernoulli beam theory and the transfer matrix method, general solutions in the periodic part of beam are obtained. It is shown that when the eigenfrequencies of the beam free vibrations coincide with the stopband frequencies of counterpart infinite beam, a strong localization of beam slopes and moments occur at the first interface of the periodic part of beam. The electrical voltage generating by the piezoelectric patch is proportional to the slopes of the beam periodic structure. The maximal harvesting energy occurs at stopband eigenfrequencies, at which the beam slope strong localization takes place.

Introduction. Vibration-based energy harvesting is a growing modern area for generating low-power electricity to use in wireless electronic devices, such as portable electronics and wireless sensors. In recent years efficient electrical energy generation and harvesting have become one of the most practical topics in engineering research. Energy storage devices come in many designs, with piezoelectric energy storage being especially common. These devices utilize the property of piezoelectric materials to generate an electric field when mechanical force is applied. Vibration-based energy harvesting is a modern method for generating low-power electricity for portable electronics and wireless sensors. The fundamental research [1] provides a comprehensive study of electromechanical modeling for piezoelectric energy harvesting, including extensive case studies with experimental validations. It covers various applied models of beams with piezoelectric patch, forms of excitation in piezoelectric energy harvesting, ranging from airflow excitation to moving loads. The paper [2] provides an extensive review of contemporary piezoelectric energy harvesting techniques. It examines methods for optimizing the energy harvested from piezoelectric materials [2-8] and emphasizes successful applications [9-12]. A new type of arch beam piezoelectric stack energy harvester for railway systems is studied in paper [13]. Through simulation analyses and experimental verification of the energy harvester, the influences of external resistance, load, pre-stress, and load frequency on the energy harvesting performance of the piezoelectric energy harvester are discussed. In [14], the proposed energy harvesting device is designed as a piezoelectric cantilever beam utilizing various piezoelectric materials in both bimorph and unimorph configurations. The analytical model is derived from Euler-Bernoulli beam theory and its performance is validated against existing experimental results of piezoelectric energy harvesters in different configurations.

In work [15], an electromechanical coupled distributed-parameter model of the cantilever energy harvester is established based on Hamilton's principle, linear constitutive equations of magnetostrictive material, and Faraday's law of electromagnetic induction. In [16], a piezoelectric energy harvester composed of a buckled beam and an extended beam with a tip mass is proposed. This study develops a mathematical model and a prototype of the energy harvester. A comprehensive overview of the application of metamaterials and phononic crystals in energy harvesting is provided in [17]. Energy harvesting from structural vibrations using multifunctional resonators based on locally resonant materials is demonstrated in [18]. These structures exhibit a stop band for elastic wave propagation, with the band gap frequency determined by the microstructure's local resonance frequency.

Paper [19] presents a multifunctional structural combining superior mechanical wave filtering properties and energy harvesting capabilities. It is based on the ability of periodic structures to block elastic waves within phononic bandgaps. Energy is harvested by converting localized kinetic energy into electrical energy through the piezoelectric effect. The study presented in reference [20] employs the generalized Bloch theorem to model piezo-embedded negative mass metamaterials, demonstrating their dual functionality. It estimates power harvested by internal resonating units using resistive and shunted inductor energy harvesting circuits for a finite number of these units. The study in [21] examines the energy input/output of a composite plate with piezoelectric patches used as sensors, actuators, or energy harvesters. It concludes that there is always an optimal patch location for maximum energy transfer, regardless of frequency. For vibrational loading, energy transfer is highly sensitive to whether the operating frequency is below or above the system's resonance frequency.

This paper addresses the free vibrations of cantilever or clamped beams with periodically arranged external supports, partially covered by bonded piezoelectric patches. The periodic supports turn the multi-span beam into a collector of piezoelectric energy. Significant localization of beam slopes and moments occurs when eigenfrequencies fall within the bandgaps of a counterpart infinite beam. Energy harvested by the piezoelectric patch is highly dependent on the operating frequency, with "stopband" eigenfrequencies yielding much greater energy than "passband" frequencies.

The dynamics and stability of finite or infinite beams, supported by periodically arranged external supports analyzed by using the Euler-Bernoulli beam theory, are explored in several works by the authors of this article [22-26].

Statement of the problem

Consider a Euler- Bernoulli homogeneous beam of L length in $x \in (0, L)$. The beam in the region $x \in (a; L)$, $L = a + Nd$ is rested on N intermediate external supports periodically arranged at points $x = a + (n-1)d$, $n = 1; 2; \dots; N$. In the region $x \in (a; a + nd)$ the beam on its traction free surface is partially covered by the perfectly bonded piezoelectric patch of nd length. The beam end $x = 0$ is clamped or free, the end $x = L$ is clamped, Fig. (1)

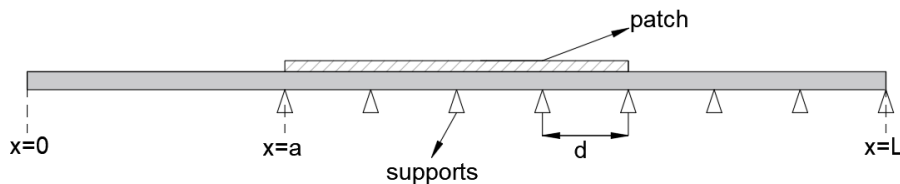


Fig 1. Beam with periodically arranged N intermediate external supports and piezoelectric patch

The equation of motion of Euler- Bernoulli beam can be cast as

$$\frac{EI}{\rho A} \frac{\partial^4 W_j}{\partial x^4} + 2\varepsilon \frac{\partial^2 W_j}{\partial t} + \frac{\partial^2 W_j}{\partial t^2} = 0; \quad (1)$$

where $W_j(x,t)$ is the deflection of the beam, E is the elastic modulus, I is the moment of inertia, ρ is the bulk density and A is the cross-sectional area of the beam, ε is the internal dumping coefficient, subscript $j=1$ denotes the region $x \in (0, a)$, subscript $j=2$ denotes the region $x \in (a, L)$.

For the beam clamped at $x = L$

$$W_2(L,t) = 0, \quad \frac{\partial W_2(L,t)}{\partial x} = 0 \quad (2)$$

two alternative boundary conditions at $x = 0$ will be considered

$$W_1(0,t) = 0 \quad \frac{\partial W_1(0,t)}{\partial x} = 0, \quad (3)$$

$$\frac{\partial^2 W_1(0,t)}{\partial x^2} = 0, \quad \frac{\partial^3 W_1(0,t)}{\partial x^3} = 0 \quad (4)$$

Assuming $W_j(x,t) = U_j(x) \cdot \exp(-\varepsilon t) \cdot \cos\left(t\sqrt{\omega^2 - \varepsilon^2}\right)$, where $U_j(x)$ is the amplitude function, ω is the vibration frequency we get

$$\frac{d^4 U_j}{dx^4} - p^4 U_j = 0, \quad p^4 = \frac{A\rho\omega^2}{EI}, \quad (5)$$

$$U_j(x) = C_{j1} \sin(px) + C_{j2} \sinh(px) + C_{j3} \cos(px) + C_{j4} \cosh(px)$$

At the beam interfaces where the external supports are placed the beam deflections are equal to zero, the moments and slopes are continuous.

At the beam interface $x = a$ we have the following conditions

$$W_1(a,t) = 0, \quad W_2(a,t) = 0 \quad (6)$$

$$\frac{\partial^2 W_1(a,t)}{\partial x^2} = \frac{\partial^2 W_2(a,t)}{\partial x^2}, \quad \frac{\partial W_1(a,t)}{\partial x} = \frac{\partial W_2(a,t)}{\partial x} \quad (7)$$

The solutions (5) in region $x \in (0, a)$ satisfying (6) and (3), (4) for clamped or cantilever beams, can be written as follows

$$U_1(x) = C_{11} (\sinh(ap) \sin(px) - \sin(ap) \sinh(px)) + C_{12} (\sinh(ap) (\cos(px) + \gamma \cosh(px)) - \sinh(px) (\cos(ap) + \gamma \cosh(ap))) \quad (8)$$

Here and hereinafter, $\gamma = 1$ corresponds to the cantilever beam, $\gamma = -1$ to the clamped beam.

Solutions in the periodic structure, transfer matrix approach

In the periodically arranged structure we consider solutions in the basic unit cell $x \in (\beta_{n-1}, \beta_n)$; $\beta_n = a + nd$, $n = 1; 2; \dots N$. (9)

interface conditions at points where the supports are located can be cast as

$$U_2(\beta_n) = 0, \quad \left[\frac{dU_2(\beta_n)}{dx} \right] = 0, \quad \left[\frac{d^2U_2(\beta_n)}{dx^2} \right] = 0 \quad (10)$$

Here $[*]$ is a jump of a function across the interfaces.

In the basic unit cell, the solutions for the amplitude functions (5) that satisfy the conditions (10) can be determined as follows:

$$U_2(x) = C_{21} \left[\sin(p(\beta_{n-1} - x)) + \sin(dp) \cdot \cosh(p(\beta_n - x)) - \cosh(dp) \cdot \sin(p(\beta_n - x)) \right] + C_{22} \left[\sinh(dp) \sin(p(\beta_n - x)) - \sin(dp) \sinh(p(\beta_n - x)) \right] \quad (11)$$

Since the interface contact conditions are imposed on the beam slope $\psi(x)$ and moment $\mu(x)$

$$\psi(x) = \frac{dU_2(x)}{dx}, \quad \mu(x) = \frac{d^2U_2(x)}{dx^2} \quad (12)$$

it is appropriate to introduce the following column vector.

$$\mathbf{U}_2(x) = \begin{pmatrix} \psi(x) \\ \mu(x) \end{pmatrix}. \quad (13)$$

Considering vector $\mathbf{U}_2(x)$ at points $x = \beta_n$; $x = \beta_{n-1}$ the following conditions are valid

$$\begin{aligned} \mathbf{U}_2(\beta_n - d) &= \mathbf{QC}, & \mathbf{U}_2(\beta_n) &= \mathbf{PC}; \\ \mathbf{U}_2(\beta_n - d) &= \mathbf{QC}, & \mathbf{U}_2(\beta_n) &= \mathbf{PC}; \end{aligned} \quad (14)$$

where

$$\mathbf{Q} = \begin{pmatrix} q[\cos(dq)\cosh(dq) - \sin(dq)\sinh(dq) - 1] & q[\sin(dq)\cosh(dq) - \cos(dq)\sinh(dq)] \\ 2q^2 \sin(dq)\cosh(dq) & -2q^2 \sin(dq)\sinh(dq) \end{pmatrix} \quad (15)$$

$$\mathbf{P} = \begin{pmatrix} q[\cos(dq)\cosh(dq) - \sin(dq)\sinh(dq) + 1] & q[\sin(dq)\cosh(dq) - \cos(dq)\sinh(dq)] \\ 2q^2 \sin(dq)\cosh(dq) & -2q^2 \sin(dq)\sinh(dq) \end{pmatrix}$$

Eliminating the vector \mathbf{C} from (14), the relation linking vector field values within the unit cell can be found as follows:

$$\mathbf{U}_2(\beta_n) = \mathbf{M}\mathbf{U}_2(\beta_{n-1}); \quad \mathbf{M} = \mathbf{P}(\beta_n)\mathbf{P}^{-1}(\beta_{n-1}). \quad (16)$$

The unimodal propagator matrix \mathbf{M} herein connects the field vectors at the end points of the n -th cell.

$$\mathbf{M} = \begin{pmatrix} \frac{\sin(dp)\cosh(dp) - \cos(dp)\sinh(dp)}{\sin(dp) - \sinh(dp)} & \frac{1 - \cos(dp)\cosh(dp)}{p(\sin(dp) - \sinh(dp))} \\ \frac{2p\sin(dp)\sinh(dp)}{\sin(dp) - \sinh(dp)} & \frac{\sin(dp)\cosh(dp) - \cos(dp)\sinh(dp)}{\sin(dp) - \sinh(dp)} \end{pmatrix} \quad (17)$$

Repeating this procedure n times determines the propagator unimodal matrix \mathbf{M}^n .

The matrix \mathbf{M}^n for any $n = 1; 2; \dots; N$ links the vectors at points of the beam

$$\mathbf{U}_2(a + nd) = \mathbf{M}^n \mathbf{U}_2(a). \quad (18)$$

Taking into account that $\mathbf{M}^{N-n} \mathbf{U}_2(a + nd) = \mathbf{U}_2(a + Nd) = \mathbf{U}_2(L)$ we can link the vectors at beam $x = L$ and $x = a + d(n-1)$ points in the following way

$$\mathbf{U}_2(L) = \mathbf{M}^{N-n+1} \mathbf{U}_2(a + d(n-1)). \quad (19)$$

At the clamped edge $x = L$ we have

$$\mathbf{U}_2(L) = \begin{pmatrix} 0 \\ \mu(L) \end{pmatrix}. \quad (20)$$

Here $\mu(L)$ is uncertain value of the beam moment at the clamped end.

According to Sylvester's matrix polynomial theorem [27] for 2×2 matrices the elements of the n -th power of an unimodal matrix \mathbf{M}^n can be cast as

$$\mathbf{M}^n = \begin{pmatrix} M_{11}(n) & M_{12}(n) \\ M_{21}(n) & M_{22}(n) \end{pmatrix} \quad (21)$$

$$M_{11}(n) = m_{11}S_{n-1}(\eta) - S_{n-2}(\eta), M_{12}(n) = m_{12}S_{n-1}(\eta),$$

$$M_{21}(n) = m_{21}S_{n-1}(\eta), M_{22}(n) = m_{22}S_{n-1}(\eta) - S_{n-2}(\eta)$$

where $S_n(\eta)$ are the Chebyshev polynomials of second kind, namely

$$S_n(\eta) = \frac{\sin((n+1)\arccos(\eta))}{\sin(\arccos(\eta))}; \quad \eta = \frac{1}{2} \text{tr}(\mathbf{M})$$

On the other hand, according to Bloch equation

$$\cos(kd) = \eta(\omega) \quad (22)$$

the function $\eta(\omega)$ defines the frequencies of bandgaps of the counterpart infinite beam,

k is the Bloch wave number [26].

From (22) it follows that conditions $|\eta(\omega)| < 1$, $|\eta(\omega)| > 1$ define passband" and stopband frequencies in the counterpart infinite beam, respectively.

In vector notations we can write the interface condition at point $x = a$ as

$$\mathbf{U}_2(a) = \mathbf{U}_1(a) \quad (23)$$

Using (8), we can find

$$\mathbf{U}_2(a) = \begin{pmatrix} pC_{11}(\cos(ap)\sinh(ap) - \sin(ap)\cosh(ap)) - \\ -pC_{12}(\sin(ap)\sinh(ap) + \cos(ap)\cosh(ap) + \gamma) \\ -2p^2\sinh(ap)(C_{11}\sin(ap) + C_{12}\cos(ap)) \end{pmatrix} \quad (24)$$

Considering equations (16) and (23), we obtain the following matrix equation that determines the unknown constants C_{11}, C_{12}

$$\begin{pmatrix} M_{11}(N) & M_{12}(N) \\ M_{21}(N) & M_{22}(N) \end{pmatrix} \mathbf{U}_2(a) = \mathbf{U}_2(L) \quad (25)$$

Taking into account (18) and solving this matrix equation we find constants C_{11}, C_{12}

$$C_{11} = -\frac{\mu(L) \cdot M_{11}(N) \cdot [\sin(ap) + \gamma \text{csch}(ap) + \cos(ap) \text{coth}(ap)]}{2p^2(\gamma \sin(ap) + \text{sh}(ap))} - \frac{2p\mu(L) \cdot M_{12}(N) \cos(ap)}{2p^2(\gamma \sin(ap) + \text{sh}(ap))}, \quad (26)$$

$$C_{12} = \frac{\mu(L) \left(-M_{11}(N) (\cos(ap) - \sin(ap) \text{coth}(ap)) + 2pM_{12}(N) \sin(ap) \right)}{2p^2(\gamma \sin(ap) + \text{sh}(ap))}$$

Here $\mu(L)$ is an uncertain moment constant.

Substituting (26) into (24) gives us the beam slope and moment at a point $x = a$ clamped and cantilever beams

Substituting (26) into (24) gives the beam slope and moment at a point $x = a$

$$\begin{aligned}\psi(a) &= \mu(L)M_{12}(N), \\ \mu(a) &= \mu(L)M_{22}(N)\end{aligned}\quad (27)$$

On the other hand, as It follows from (19) that for any $n = 1; 2; \dots; N$

$$\begin{pmatrix} \psi(\beta_m) \\ \mu(\beta_m) \end{pmatrix} = \begin{pmatrix} M_{12}(m)\mu(L) \\ M_{22}(m)\mu(L) \end{pmatrix}; \quad m = N - 1 + n \quad (28)$$

Based on (25) and (26), the relative slope and moments at any unit cell of the periodic part of the beam can be defined as follows.

$$\begin{aligned}\tilde{\psi}_n &= \frac{\psi(a + d(N - n + 1))}{\psi(a)} = \frac{M_{12}(N - n + 1)}{M_{12}(N)} = \frac{S_{N-n}(\eta)}{S_{N-1}(\eta)} \\ \tilde{\mu}_n &= \frac{\mu(a + d(N - n + 1))}{\mu(a)} = \frac{M_{22}(N - n + 1)}{M_{22}(N)} = \frac{T_{N-n+1}(\eta)}{T_N(\eta)}\end{aligned}\quad (29)$$

where $T_n(\eta)$ is the Chebyshev polynomials of first kind.

From non-triviality condition of eigenfunctions ($\mu(L) \neq 0$) and boundary conditions (2) and (3) at $x = 0$ that have not yet been used, we derive the following the following different equations defining eigenfrequencies for clamped and cantilever beams

$$\begin{aligned}\Delta(\omega) &= M_{11}(N)(\gamma \operatorname{csch}(ap) + \cos(ap) \operatorname{coth}(ap)) + \\ &+ pM_{12}(N)(\cos(ap) - \sin(ap) \operatorname{coth}(ap))\end{aligned}\quad (30)$$

Here, as previously indicated $\gamma = 1$ corresponds to the cantilever beam, whereas $\gamma = -1$ to the clamped beam,

For a of beam without periodic supports ($d \rightarrow 0$) of length a , the eigenfrequency equations for clamped and cantilever beams can be derived from the following equation

$$\Delta_0(\omega) = (\gamma \operatorname{csch}(ap) + \cos(ap) \operatorname{coth}(ap)) \quad (31)$$

Piezoelectric patch under flexural vibration of the beam

The equations and relationships for a piezoelectric patch perfectly bonded with elastic beam provided here are based on [1].

A uniform composite Euler–Bernoulli covered in the region $x \in (a, a + nd)$ by a perfectly bonded uniform piezoelectric patch, which the top and bottom surfaces are metalized by thin electrodes of negligible thicknesses. The electrodes bracketing the piezoelectric layers are connected to a resistive electrical circuit.

The piezoelectric patch is operating in (31) mode which means that the poling direction of the piezoelectric material of patch is perpendicular to the beam centerline, “1” and “3”

directions are coincident with x and z directions, respectively “1” is the direction of axial strain and “3” is the direction of polarization.

The constitutive relations for piezoelectric patch in (31) mode are

$$\xi_1(x, z, t) = Y^{-1}\sigma_1(x, z, t) + d_{31}E_3(x, z, t) \quad (32)$$

$$D_3(x, z, t) = d_{31}\sigma_1(x, z, t) + \epsilon_{33}^T E_3(x, z, t) \quad (33)$$

Here $\xi_1(x, z, t)$, $\sigma_1(x, z, t)$ are the axial strain and stress arising in the patch due to bending of beam, $E_3(x, z, t)$ the electric field, $D_3(x, z, t)$ the electric displacement, d_{31} is the piezoelectric coefficient, ϵ_{33}^T is permittivity in direction of the polarization axis measured at constant mechanical stress, Y is the Young's moduli of patch material.

From (36) the expression for the stress $\sigma_1(x, z, t)$ can be written as

$$\sigma_1(x, z, t) = Y(\xi_1(x, z, t) - d_{31}E_3(x, z, t)) \quad (34)$$

Substituting (34) in (33) yields

$$D_3(x, z, t) = e_{31}\xi_1(x, z, t) + \epsilon_{33}^S E_3 \quad (35)$$

where $e_{31} = Yd_{31}$, $\epsilon_{33}^S = (\epsilon_{33}^T - d_{31}e_{31})$, ϵ_{33}^S is the permittivity of piezoelectric material measured at constant strain.

The average bending strain in the in uniform piezoelectric patch can be expressed as

$$\xi_1(x, z, t) = -h_c \frac{\partial^2 W(x, t)}{\partial x^2}, \quad (36)$$

where $W(x, t)$ is transverse displacement of the beam's centerline, h_c is the distance of the center of the piezo layer in thickness direction to the beam centerline.

Taking into account that the uniform electric field in terms of the electric potential difference is

$$E_3 = v(t)/h_p, \quad (37)$$

where $v(t)$ is voltage across the resistive load r , h_p is the thickness of patch the and using (35) the following equation can be obtained

$$D_3(x, z, t) = -e_{31}h_c \frac{\partial^2 W(x, t)}{\partial x^2} - \frac{\epsilon_{33}^S}{h_p} v(t). \quad (38)$$

Assuming that the electrodes of the piezoceramic patch are connected to a resistive electrical load r , the integral form of Gauss's law can be applying as

$$\frac{d}{dt} \left(\int_A \mathbf{D} \mathbf{n} dA \right) = \frac{v(t)}{r}. \quad (39)$$

Here, \mathbf{D} is the vector of electric displacement, \mathbf{n} is the unit outward normal, and the integration is performed over the electrode area A of the piezoceramic patch.

Since in our case contribution to the inner product of the integrand in equation (39) is $D_3(x, z, t)$ we can rewrite (39) as

$$\frac{d}{dt} \left(\int_A \mathbf{D} \mathbf{n} dA \right) = b \int_a^{a+nd} \frac{d}{dt} (D_3(x, z, t)) dx = \frac{v(t)}{r}, \quad (40)$$

where $a + nd$ is the length and b is the width of the patch.

From (37) and (40) we get the following equation for voltage function $v(t)$

$$\begin{aligned} v(t) + f \frac{dv(t)}{dx} &= -g \left(\frac{\partial W(a+nd, t)}{\partial x \partial t} - \frac{\partial W(a, t)}{\partial x \partial t} \right) = \\ &= g F_0 e^{-t\epsilon} \left(\sqrt{\omega^2 - \epsilon} \sin(t\sqrt{\omega^2 - \epsilon}) + \epsilon \cos(t\sqrt{\omega^2 - \epsilon}) \right) \end{aligned} \quad (41)$$

$$F_0 = \psi(a+nd) - \psi(a); \quad f = \frac{dn b \epsilon_{33}^S r}{h_p}; \quad g = e_{31} h_c b r$$

The solution for function $v(t)$ under condition $v(0) = 0$ can be find as

$$\begin{aligned} v(t) &= \frac{F_0 g \left(f \sqrt{\omega^2 - \epsilon^2} \sin(t\sqrt{\omega^2 - \epsilon^2}) + (f\epsilon - \omega^2) \cos(t\sqrt{\omega^2 - \epsilon^2}) \right) e^{-\epsilon t}}{f^2 - 2f\epsilon + \omega^2} - \\ &- \frac{F_0 g (f\epsilon - \omega^2) e^{-f t}}{f^2 - 2f\epsilon + \omega^2} \end{aligned} \quad (42)$$

From (42) it follows that the electrical voltage generated by the piezoelectric patch is proportional to the function F_0 that depends of the slopes of the beam's periodic part.

Analysis and conclusions.

From (22) it follows that condition $|\eta| > 1$ defines the bandgaps of counterpart infinite beam.

The Fig.2 shows the deviation function $|\eta(\Omega)|$ versus non-dimensional frequency

$$\Omega = \omega d^2 \sqrt{(EI)^{-1} \rho A} \quad \text{in the region } |\eta(\Omega)| \geq 1, 0 < \Omega < 160$$

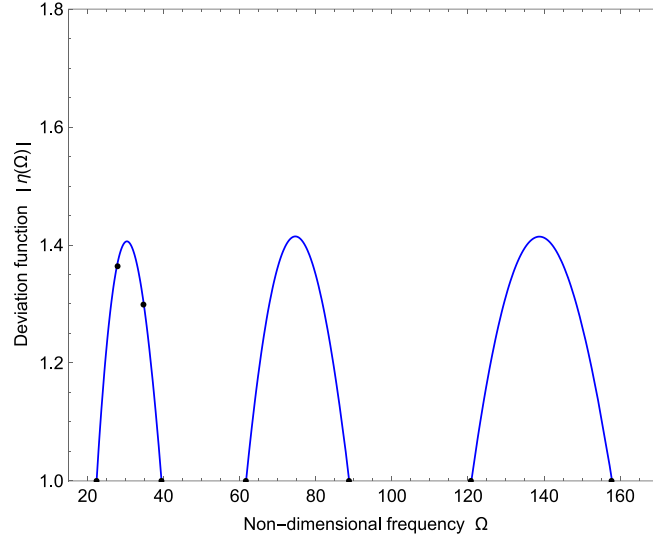


Fig 2. The graphs of the deviation function versus of non-dimensional frequency

The curves define first gap $\Omega \in (22.37, 39.43)$, the second and third gaps $\Omega \in (61.62, 88.73)$ and $\Omega \in (120.78, 157.75)$, respectively. Black points on the axes $|\eta(\Omega)| = 1$ mark the boundaries of the gaps. Points on the first bandgap curve correspond to minimal eigenfrequencies in the first gap $(\Omega_c = 34.9; \eta(\Omega_c) = 1.37)$, $(\Omega_f = 27.9; \eta(\Omega_f) = 1.32)$ of clamped and cantilever beams when $a = 5d$, respectively.

The relative slope is given by the formula $\tilde{\psi}_n = S_{N-n}(\eta) / S_{N-1}(\eta)$;

In Fig. 3 the graphs of relative discrete slope function \tilde{s}_n versus of the number of supports are presented in the case $a = 5d$; $N = 5$; $N = 10$. The blue plots are calculated for clamped beam at eigenfrequency Ω_c , while the red plot is calculated for clamped beam at beam at eigenfrequency Ω_f (see Fig.2).

Evidently, similar graphs can be plotted for relative slopes and moment functions at any stopband eigenfrequency.

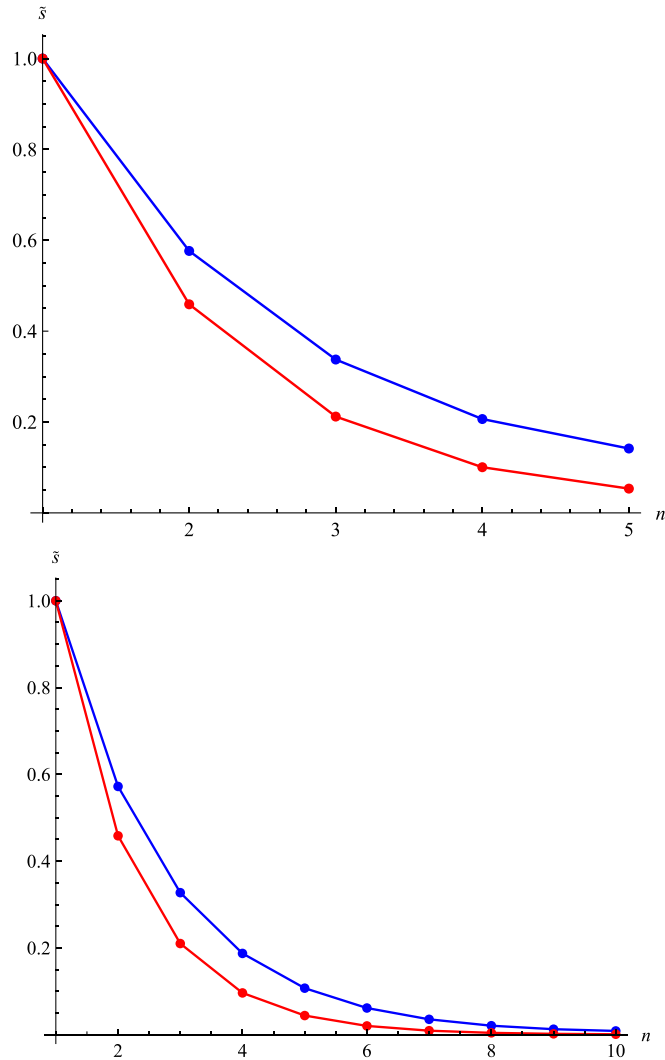


Fig.3 The graphs of discrete slope functions \tilde{s}_n within first band gap versus support numbers

Analysis of these curves reveals that the localization of beam slope significantly increases with increasing number of supports. The results demonstrate that flexible waves, defined by beam slopes and moments, are unable to propagate through periodic structures at frequencies within the bandgaps of a counterpart infinite beam. Instead, they localize near the first periodic cell, reaching a maximum value at $x = a$. This effect is noticeable at $N = 5$.

Fig. 4. confirms that localization of the slope and moments does not occur at the eigenfrequencies outside of the bandgaps.

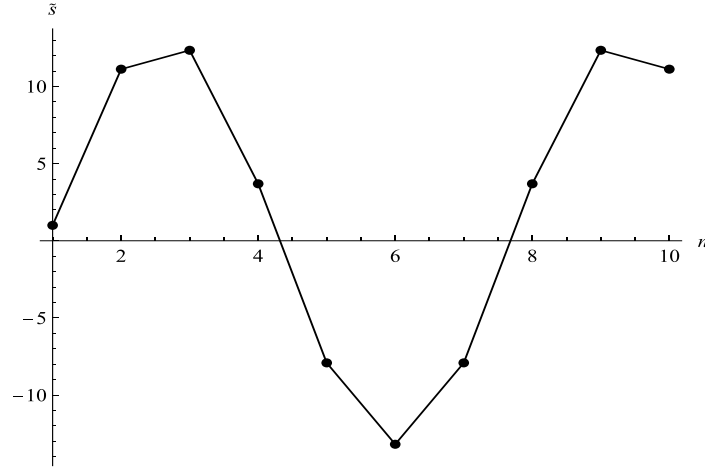


Fig 4. The graph of discrete slope function \tilde{s}_n outside of bandgaps

Figures 5 and 6 display the graphs of the function $\Delta(\Omega)$ whose zeros determine the eigenfrequencies. The black markers on the axis Ω represent the boundaries of the gaps. The graphs of the function $\Delta(\Omega)$ are presented within the range $0 < \Omega < 200$ for $N = 10$ and $N = 30$ for clamped (blue curves) and cantilever (red curves) beams when $a = 5d$. Figures 5 and 6 demonstrate that adding more supports increases eigenfrequencies outside bandgaps but does not affect the zero locations within bandgaps. Few eigenfrequencies exist within these gaps. When $a < 5d$, here are no zeroes of the function $\Delta(\Omega)$ in bandgaps, the eigenfrequencies remain outside the bandgaps.

In Fig.7 the graphs of function $\Delta(\Omega)$ of the clamped and cantilever beams presented within the range of first bandgap, when $a = 5d$; $N = 10$.

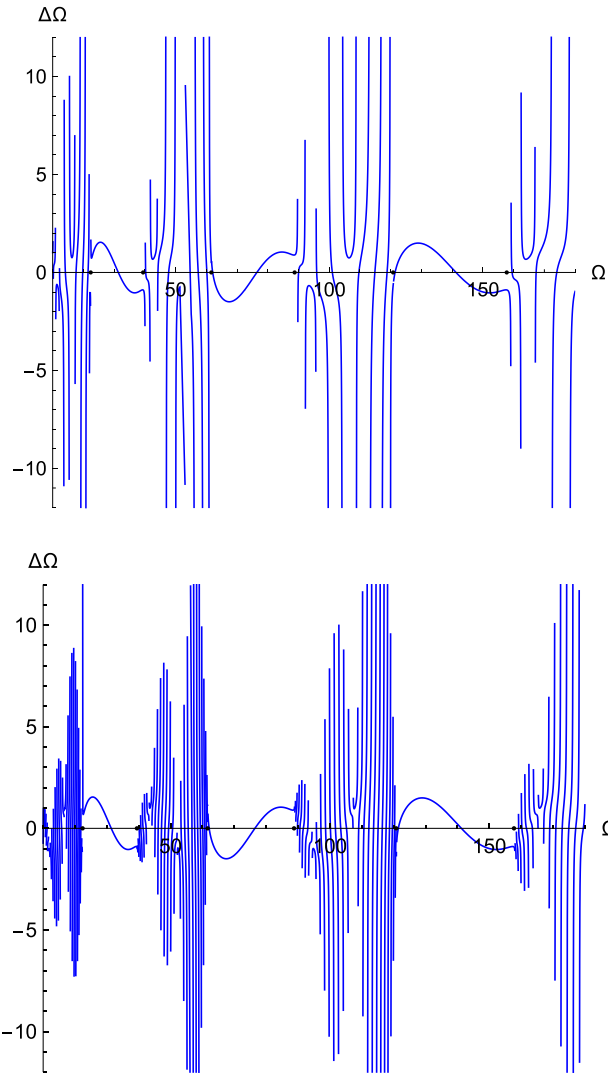


Fig.5 The graphs of function $\Delta(\Omega)$ of the clamped beam presented within the range $0 < \Omega < 200$, $a = 5d$; $N = 10$; $N = 30$.

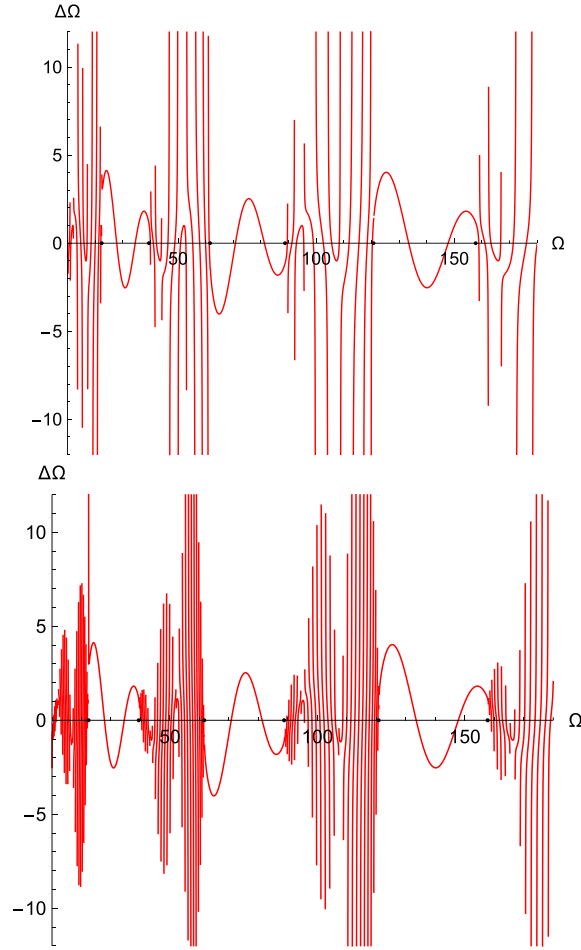
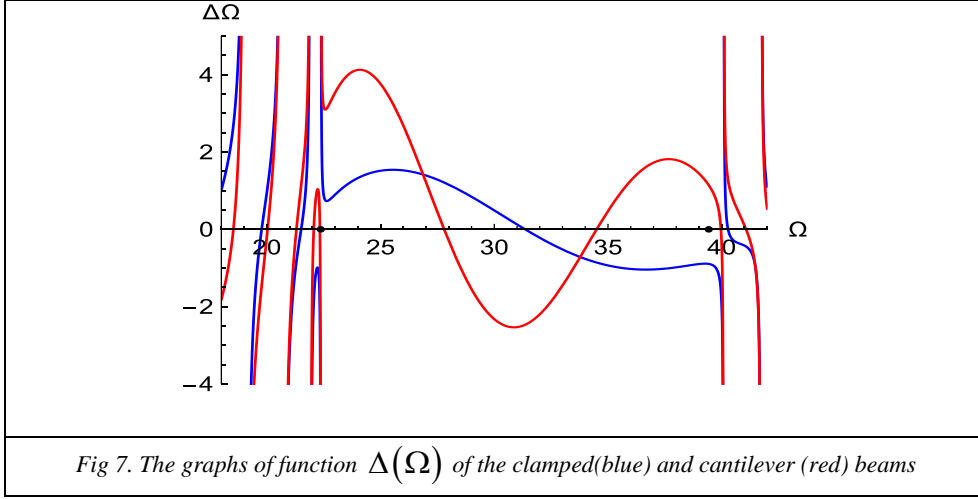


Fig.6 The graphs of function $\Delta(\Omega)$ of the cantilever beam , presented within the range $0 < \Omega < 200$, $a = 5d$; $N = 10$; $N = 30$,

According (42) the electrical voltage generated by the piezoelectric patch of nd length due to beam vibration is proportional to function $F_{0n} = (\psi(a) - \psi(a + nd))$.

When the beam eigenfrequencies are within the bandgaps, the function $\psi(a + nd)$ at these frequencies approaches zero monotonously at $n \rightarrow N$ (See Fig.3). Therefore, the function $F_{0n} = (\psi(a) - \psi(a + nd))$ is maximal when $n = N$.



This indicates that the maximum impact of the piezoelectric patch occurs when a patch of length L covers the entire periodic part of the beam.

Considering (27), the function F_{0n} versus beam flexural frequency can be expressed as

$$F_{01}(\Omega_j) = \frac{\mu(L)(1 - \cos(\sqrt{\Omega_j}) \cosh(\sqrt{\Omega_j}))}{\sqrt{\Omega_j}(\sin(\sqrt{\Omega_j}) - \sinh(\sqrt{\Omega_j}))} (S_{N-1}(\eta(\Omega_j)) - S_{N-2}(\eta(\Omega_j)))$$

where Ω_j are the beam eigenfrequencies.

For estimation of the effect of the beam slope on harvesting energy, consider the following relative function

$$F_{*N}(\Omega_1, \Omega_2) = \frac{F_{01}(\Omega_1)}{F_{01}(\Omega_2)}$$

Here $\Omega_1 = 27.9$ is the “stopband” eigenfrequency of cantilever beam in the first gap,

$\Omega_2 = 21.5$ is the nearest to Ω_1 the “passband” eigenfrequency.

At these eigenfrequencies when $a = 5d$, $N = 5$, $N = 10$, $N = 20$ we have respectively

$$F_{*5} \approx 22.2, F_{*10} \approx 440.5, F_{*20} \approx 1410.8.$$

The same estimation applies to any stopband and passband eigenfrequencies. The generated harvesting energy depends heavily on the operating frequency, with greater effects at stopband frequencies than at passband. More supports significantly increase the harvesting energy values.

The main results can be summarized as follows:

1. In the case of free vibration of a beam with periodically arranged supports, significant localization (maximization) of the beam slopes and moments occurs when the eigenfrequencies of the beam are within the bandgaps of the counterpart infinite beam.
2. Localization occurs even with a few periodically arranged supports.
3. The flexible wave of supported beam cannot travel freely through a periodic structure at frequencies within bandgaps of counterpart infinite beam and are practically localized at the neighborhood of the first periodic cell interface.
4. The number of periodically arranged supports significantly increases the number of eigenfrequencies outside of the bandgaps without changing this number within the gaps.
5. The electric voltage output of a piezo patch under beam bending is significantly influenced by the dynamic behavior of the beam's periodic structure and is proportional to the beam slopes at the locations of the periodic supports.
6. The energy harvested by a piezoelectric patch strongly depends on the operating frequency. The harvesting energy at stopband eigenfrequencies incomparable greater than at passband eigenfrequencies.

Acknowledgments

The work was supported by the State Committee of Science of RA, in the framework of the research projects 25RG-2C066, 25RG-2C136.

References

1. Erturk, A. and Inman, D.J., 2011. *Piezoelectric energy harvesting*, John Wiley & Sons, p.539, <http://dx.doi.org/10.1002/9781119991151.ch10>
2. Covaci C.; Gontean A., Piezoelectric Energy Harvesting Solutions: A Review, *Sensors*, (2020), vol.20, 3512. <https://doi.org/10.3390/s20123512>,
3. Liu, H.; Hua, R.; Lu, Y.; Wang, Y.; Salman, E.; Liang, J. Boosting the efficiency of a footstep piezoelectric-stack energy harvester using the synchronized switch technology. *Journal of Intelligent Material Systems and Structures*. **2019**, *30*, 813–822, <https://doi.org/10.1177/1045389X19828512>,
4. Briscoe, J.; Dunn, S. 3.2.6 Applications. In *Nanostructured Piezoelectric Energy Harvesters*, 1st ed.; Springer International Publishing: Berlin/Heidelberg, Germany, 2014; pp. 39–42,
5. Erturk, A.; Inman, D.J. 11.1 AC-DC Rectification and Analysis of the Rectified Output. In *Piezoelectric Energy Harvesting*, 1st ed.; John Wiley & Sons: Hoboken, NJ, USA, 2011; pp. 325–331,
6. Shu, Y.C.; Lien, I.C. Analysis of power output for piezoelectric energy harvesting systems. *Smart Mater. Struct.* **2006**, *15*, 1499–1512, <https://doi.org/10.1088/0964-1726/15/6/001>

7. Guan, M.J.; Liao, W.H. On the efficiencies of piezoelectric energy harvesting circuits towards storage device voltages. *Smart Mater. Struct.* 2007, *16*, 498–505, <https://doi.org/10.1088/0964-1726/16/2/031> ,
8. Liang, J.; Liao, W. Piezoelectric Energy Harvesting and Dissipation on Structural Damping. *Journal of Intelligent Material Systems and Structures.* 2008, *20*, 515–527, <https://doi.org/10.1177/1045389X08098194>,
9. Lallart, M.; Guyomar, D. An optimized self-powered switching circuit for non-linear energy harvesting with low voltage output. *Smart Mater. Struct.* 2008, *17*, 035030, <https://doi.org/10.1088/0964-1726/17/3/035030>,
10. Edlund, C.; Ramakrishnan, S. An analytic study of vibrational energy harvesting using piezoelectric tiles in stairways subjected to human traffic. *Eur. J. Appl. Math.* 2019, *30*(5), 968–985, <https://doi.org/10.1017/S095679251800058X> ,
11. Ali A., Shaukat H., Kouritem S.A., Bibi S., Altabey W. A., Recent progress in energy harvesting systems for wearable technology, *Energy Strategy Reviews* (2023), vol. 49, 101124, <https://doi.org/10.1016/j.esr.2023.101124>,
12. Man D, Hu Q, Xu Q, Tang L, Chen D, Yuan Z, Han T. Numerical Analysis of Dynamic Characteristics of an Asymmetric Tri-Stable Piezoelectric Energy Harvester under Random Vibrations in Building Structures. *Buildings.* 2024; *14*(7):2210. <https://doi.org/10.3390/buildings14072210> .
13. Min Zh., Hou Ch., Sui G., Shan X., Xie T., Simulation and Experimental Study of a Piezoelectric Stack Energy Harvester for Railway Track Vibrations, *Micromachines*, (2023), vol.14, 892. <https://doi.org/10.3390/mi14040892>
14. Machu, Z., Rubes, O., Sevecek, O. and Hadas, Z., 2021. Experimentally verified analytical models of piezoelectric cantilevers in different design configurations. *Sensors*, *21*(20), p.6759. <http://dx.doi.org/10.3390/s21206759>
15. Wang L., Lian Ch., Shu D., Yan Z., Nie X., Analytical solution and optimal design for the output performance of Galfenol cantilever energy harvester considering electromechanical coupling effect, *Scientific Reports*, (2023), vol.13:12857 | <https://doi.org/10.1038/s41598-023-40111-x>,
16. Wen-Po Sun, Wei-Jiun Su., Design and analysis of an extended buckled beam piezoelectric energy harvester subjected to different axial preload, *Smart Mater. Struct.* **33** (2024) 055007 (14pp), <https://doi.org/10.1088/1361-665X/ad38a4>,
17. Hu, G., Tang, L., Liang, J., Lan, C. and Das, R., 2021. Acoustic-elastic meta-materials and phononic crystals for energy harvesting: A review. *Smart Materials and Structures*, *30*(8), p.085025. <https://doi.org/10.1088/1361-665x/ac0cbc/>
18. Mikoshiba, K., Manimala, J.M. and Sun, C.T., 2013. Energy harvesting using an array of multifunctional resonators. *Journal of Intelligent Material Systems and Structures*, *24*(2), pp.168-179. <http://dx.doi.org/10.1177/1045389X12460335>
19. Gonella, S., To, A.C. and Liu, W.K., Interplay between phononic bandgaps and piezoelectric microstructures for energy harvesting. *Journal of the Mechanics and Physics of Solids*, (2009),*57*(3), pp.621-633. <https://doi.org/10.1016/j.jmps.2008.11.002>

20. Dwivedi, A., Banerjee, A., Adhikari, S. and Bhattacharya, B., 2021. Optimal electromechanical bandgaps in piezo-embedded mechanical metamaterials. *International Journal of Mechanics and Materials in Design*, 17(2), pp.419-439. <https://link.springer.com/article/10.1007/s10999-021-09534-0>
21. Piliposian G ,A. Hasanyan .A, Piliposyan G. Jilavyan H, (2020), On the Sensing, Actuating and Energy Harvesting Properties of a Composite Plate with Piezoelectric Patches, *International Journal of Precision Engineering and Manufacturing-Green Technology*, Vol.7, pp. 657–668. [DOI 10.1007/s40684-020-00219-1](https://doi.org/10.1007/s40684-020-00219-1)
22. Avetisyan A.S., Belubekyan M.V., Ghazaryan K.B., Stability of a beam with periodic supports, *Proc. of NAS of Armenia, Mechanics*. (2015), vol. 68, № 3, pp. 16-21, <http://doi.org/10.33018/68.3.2>,
23. Avetisyan A.S., Khurshudyan As.Zh., (2021), Benchmarking the difference of moving follower and normal loads on linear and nonlinear Euler-Bernoulli and Timoshenko beams, *ZAMM- Journal of Applied Mathematics and Mechanics*, <https://doi.org/10.1002/zamm.202000350>,
24. Avetisyan A.S., Ghazaryan K., Marzocca P., Stability of a finite length multi-span beam resting on periodic rigid and elastic supports, *Int. Journal of Solids and Structures* (2023), vol. 281, 112410, <https://doi.org/10.1016/j.ijsolstr.2023.112410>,
25. Avetisyan A.S., Ghazaryan K., Marzocca P., Stability of a Multi-Span Current-Carrying Beam Resting on Periodic Supports and Exposed to an External Magnetic Field, *Journal of Applied Mechanics, ASME*, (2024), Vol. 91/061009-2, <https://doi.org/10.1115/1.4>,
26. Ghazaryan, K., Piliposyan, G., Jilavyan, S. and Piliposian, G., 2024. Forced vibrations of a finite length metabeam with periodically arranged internal hinges and external supports. *European Journal of Mechanics-A/Solids*, 103, p.105194, <https://doi.org/10.1016/j.euromechsol.2023.105194>
27. Tovar, A.A. and Casperson, L.W., 1995. Generalized Sylvester theorems for periodic applications in matrix optics. *Journal of the Optical Society of America A*, 12(3), pp.578-590. <https://doi.org/10.1364/JOSAA.12.000578>

Information about the authors:

Avetisyan Ara S. - Chief Researcher of the Institute of Mechanics of the National Academy of Sciences of Armenia, ara_avetisyan@sci.am

Kazaryan Karen B. - Chief Researcher of the Institute of Mechanics of the National Academy of Sciences of Armenia, ghkarren@gmail.com

Pier Marzocca - Sir Lawrence Wackett Centre, RMIT University, 124 La Trobe St, Melbourne VIC 3000, Australia, pier.marzocca@rmit.edu.au

Received 20 June 2025